Differential development of large-cell neuroendocrine or small-cell lung carcinoma upon inactivation of 4 tumor suppressor genes

Sara Lázaro[a,b], Miriam Pérez-Crespo[a,b,1], Corina Lorz[a,b,c,1], Alejandra Bernardini[a,b,c], Marta Oteo[d], Ana Belén Enguita[e], Eduardo Romero[d], Pilar Hernández[a], Laura Tomás[f], Miguel Ángel Morcillo[d], Jesús M. Paramio[a,b,c], and Mirentxu Santos[a,b,c,2]

[a]Molecular Oncology Unit, Centro de Investigaciones Energéticas Medioambientales y Tecnológicas (CIEMAT), 28040 Madrid, Spain; [b]Institute of Biomedical Research, University Hospital "12 de Octubre," 28041 Madrid, Spain; [c]Centro de Investigación Biomédica en Red de Cáncer (CIBERONC), 28029 Madrid, Spain; [d]Biomedical Applications and Pharmacokinetics Unit, CIEMAT, 28040 Madrid, Spain; [e]Pathology Department, University Hospital "12 de Octubre," 28041 Madrid, Spain; and [f]Department of Biochemistry, Genetics and Immunology, University of Vigo, 36310 Vigo, Spain

Edited by Harold Varmus, Weill Cornell Medical College, New York, NY, and approved September 19, 2019 (received for review December 21, 2018)

High-grade neuroendocrine lung malignancies (large-cell neuroendocrine cell carcinoma, LCNEC, and small-cell lung carcinoma, SCLC) are among the most deadly lung cancer conditions with no optimal clinical management. The biological relationships between SCLC and LCNEC are still largely unknown and a current matter of debate as growing molecular data reveal high heterogeneity with potential therapeutic consequences. Here we describe murine models of high-grade neuroendocrine lung carcinomas generated by the loss of 4 tumor suppressors. In an *Rbl1*-null background, deletion of *Rb1*, *Pten*, and *Trp53* floxed alleles after Ad-CMVcre infection in a wide variety of lung epithelial cells produces LCNEC. Meanwhile, inactivation of these genes using Ad-K5cre in basal cells leads to the development of SCLC, thus differentially influencing the lung cancer type developed. So far, a defined model of LCNEC has not been reported. Molecular and transcriptomic analyses of both models revealed strong similarities to their human counterparts. In addition, a ^{68}Ga-DOTATOC–based molecular-imaging method provides a tool for detection and monitoring the progression of the cancer. These data offer insight into the biology of SCLC and LCNEC, providing a useful framework for development of compounds and preclinical investigations in accurate immunocompetent models.

LCNEC | SCLC | cell of origin | tumor suppressor

The 2015 World Health Organization classification (1) grouped pulmonary neuroendocrine tumors (small-cell lung carcinoma, SCLC; large-cell neuroendocrine carcinoma, LCNEC; atypical carcinoma, AC; and typical carcinoma, TC) together in 1 category. SCLC and LCNEC are classified as high-grade malignancies. LCNEC is distinguished from SCLC based on cytomorphological features. With poor prognosis and no optimal treatment achieved to date, LCNEC accounts for 3% of lung cancers. SCLC accounts for 15% of all lung cancers, with a 5-y survival rate below 5% and still chemotherapy as the first-line treatment option. Additionally, the majority of patients with LCNEC and SCLC are diagnosed at advanced stages of the disease, making their therapeutic management particularly difficult. Therefore another unmet necessity in these tumors involves creating a suitable system of in vivo specific detection. The biological relationships between LCNEC and SCLC are under debate. Although they share neuroendocrine differentiation, immunohistochemical markers, aggressive behavior, and clinicopathological features, emerging molecular data from genomic profiling and next generation sequencing point to LCNEC as a heterogeneous set of diseases comprising different molecular subsets. Currently, these controversial data (2–4) raise the question of the same shared cell of origin and its role in the initiation of both types of tumors.

Mammalian lungs are constituted by the airways (trachea, bronchi, bronchioles) and alveoli (all of which are maintained during homeostasis by their own pool of stem cells) (5). Alveoli are composed of alveolar type 1 and 2 cells, and bronchioles are formed by secretory club and ciliated cells, with very scarce neuroendocrine (NE) cells. Trachea and bronchi are lined with a pseudostratified epithelium consisting of basal, secretory club, ciliated, and NE cells. Basal cells, known for the expression of keratin 5, have the ability to self-renew and directly give rise to the other epithelial cell types (6, 7). Lung squamous cell carcinoma arises from these basal cells (8). Defined mouse models of lung cancer have also revealed that SCLC arises mostly from the NE cells and from other cell types, albeit at a much lower rate (9).

Noninvasive in vivo molecular imaging using different radiotracers has greatly contributed to accurate tumor identification. ^{18}F-fluorodeoxyglucose (^{18}F-FDG) positron emission tomography (PET) has been used for the assessment of neuroendocrine tumors. However, these tumors express a high density of surface somatostatin receptors (SSTR), allowing imaging with radiolabeled somatostatin analogs. Newer PET analogs such as

Significance

High-grade neuroendocrine tumors (large-cell neuroendocrine cell carcinoma, LCNEC, and small-cell lung carcinoma, SCLC) are recalcitrant cancers for which more effective treatments and follow-up detection systems are urgently needed. Moreover, the relationship between LCNEC and SCLC is largely unknown and a current matter of debate. Human material is scarcely available, making animal models of pivotal importance. Here we report 2 robust models of LCNEC and SCLC remarkably similar to their human counterparts. We show that SCLC can arise from basal cells, which determines the evolution of the high malignant neuroendocrine lung tumor type. Besides, we provide a noninvasive imaging method based on Ga-DOTATOC to monitor changes and assess evaluation of the diseases.

Author contributions: C.L., J.M.P., and M.S. designed research; S.L., M.P.-C., M.O., E.R., P.H., and M.S. performed research; L.T. and M.S. contributed new reagents/analytic tools; S.L., M.P.-C., C.L., A.B., M.O., A.B.E., E.R., M.Á.M., J.M.P., and M.S. analyzed data; and C.L., A.B., M.O., M.Á.M., J.M.P., and M.S. wrote the paper.

The authors declare no competing interest.

This article is a PNAS Direct Submission.

Data deposition: Data related to this paper have been deposited in the Sequence Read Archive (SRA) database (accession no. PRJNA507341) and Gene Expression Omnibus (GEO) database (accession no. GSE121574).

[1]M.P.C. and C.L. contributed equally to this work.

[2]To whom correspondence may be addressed. Email: mirentxu.santos@ciemat.es.

This article contains supporting information online at www.pnas.org/lookup/suppl/doi:10.1073/pnas.1821745116/-/DCSupplemental.

First published October 14, 2019.

^{68}Ga-DOTA-peptides show higher sensitivity for tumor detection (10, 11). Therefore, in addition to conventional imaging, SSTR-targeted imaging could be applied to detect and functionally characterize neuroendocrine tumors.

Mutations in *TP53* and *RB1* are characteristic of human SCLC and LCNEC; *PTEN* alterations have been identified in SCLC (4, 12). Thus, mouse models of SCLC have been generated by deletion of these genes in different lung compartments. *RBL1* mutations have been found in 3.64% of SCLC (12). As we have previously shown the tumor suppressor activities of *Rbl1* in other tumoral types (13–15), we now interrogate the role of *Rbl1* in the development of high-grade neuroendocrine lung carcinoma. In this study, we have used a 4 tumor suppressor-based, quadruple knock out (QKO) mouse model that upon cre-mediated recombination in an *Rbl1*-null background results in the additional ablation of *Rb1*, *Pten*, and *Trp53* in adult lungs. Combined ablation of these genes leads to the development of high-grade malignant neuroendocrine lung carcinomas strikingly similar to human disease. Our results indicate that induction of the same genetic alterations in different cell types produces different tumor types and that keratin 5 expressing basal cells have the ability to give rise to SCLC. We have taken advantage of the models generated to develop a noninvasive in vivo diagnosis and follow-up system of the neuroendocrine lesions developed.

Results

Targeting Widely Versus Specifically Epithelial Cells in the Lung. Adeno-cre intratracheal infection has proven to be a robust method of modeling lung cancer in mice (16). We used 2 different approaches: on the one hand we used conventional cytomegalovirus promoter, Ad5-CMVcre, which targets most lung cell types (17) (*SI Appendix*, Fig. S1 *A–E*); on the other hand, we used an adenovirus (Ad5-K5cre) in which cre recombinase is under the control of keratin K5 promoter (18). This approach is based on the ability of proximal airway basal cells to self-renew and give rise to other cellular types (6, 7, 19) and has been reported to target lung basal cells (8). Cre activity was traced using reporter ROSA26R-tdTomato (20) and ROSA26R-LacZ mice (21) in the absence of any stimuli. Immunostaining with an antikeratin K5 antibody showed coexpression with tdTomato protein in scattered basal cells, mainly in bronchi of Ad5-K5cre–infected animals (*SI Appendix*, Fig. S1 *A′–E′*). Colocalization with lacZ confirmed basal cell cre recombination (*SI Appendix*, Fig. S1 *A″–E″*). In contrast to Ad5-K5cre targeting (*SI Appendix*, Fig. S1 *B′–E′* and *B″–E″*), Ad5-CMVcre shows coexpression with other markers of lung lineage (alveolar-, club-, or neuroendocrine-type cells) (*SI Appendix*, Fig. S1 *B–E*).

Wide Versus Specific Ablation of 4 Tumor Suppressor Genes (*Rb1*, *Rbl1*, *Pten*, and *Trp53*) in Lungs. Next, we infected adult $Rb1^{F/F}$;$Rbl1^{-/-}$;$Trp53^{F/F}$;$Pten^{F/F}$ mice with Ad5-CMVcre (CMV-QKO mice) or Ad5-K5cre (K5-QKO mice) (Fig. 1*A*). Both groups of mice developed lung tumors (87 and 84%, respectively). Most CMV-QKO mice ($n = 67$) had to be killed within 2 to 3 mo because of tumor burden, as they developed lung tumors with a median survival of 11 wk. K5-QKO mice were killed within 4 to 5 mo after Ad5-K5cre infection ($n = 67$; median survival, 17 wk) (Fig. 1*B*). None of the control mice ($n = 30$) developed any lesion. Tumor genotyping by PCR revealed the ablation of *Rb*, *Trp53*, and *Pten* and the absence of *Rbl1*, further confirmed by RT-qPCR and immunohistochemistry (*SI Appendix*, Fig. S2).

We observed that 57% of the tumors developed in the CMV-QKO mice (total number of tumors, $n = 886$; mean number of tumors per mouse, mean ± SEM = 13.42 ± 1.65) (Fig. 1*C*, *SI Appendix*, Fig. S3, and Dataset S1) shared morphological traits with human LCNEC (Fig. 1*D*), such as large cell size, abundant cytoplasm, frequent presence of nucleoli, and neuroendocrine morphology (Figs. 1*D* and 2*B*). In 6 out of 67 cases we also observed adenocarcinomas in addition to neuroendocrine tumors (*SI Appendix*, Table S1). Strikingly, in the Ad5-K5cre–infected group a different tumor spectrum was detected. In K5-QKO mice, 79% of the tumors developed (total number of tumors, $n = 537$; mean ± SEM = 8.01 ± 1.35) (Fig. 1*C*, *SI Appendix*, Fig. S3, and Dataset S1) were characterized by small-size cells with scant cytoplasm (see Figs. 1*D*, 2*C*, and 4*C*), resembling human SCLC. These findings were further confirmed by immunohistochemical expression of markers in parallel with human LCNEC and SCLC (positive Chromoganin A, TTF1, and CGRP [Fig. 1*D*] and negative CC10 and proSPC expression [not shown]).

No significant differences in tumor size were observed at median survival time for each model (*SI Appendix*, Fig. S3*B*). CMV-QKO and K5-QKO tumors were characterized by high proliferation, scattered expression of cyclin D1, absence of p19, and activation of Stat3 and Akt (Fig. 2*A*). Notably, tumors in both groups were negative for keratin 5 expression, indicating that during tumor progression after inactivation of the targeted tumor suppressor genes, tumor cells evolve lacking some of their initial characteristics. Nonetheless, according to the initial targeted cell type, we observed a different localization in the lung: CMV-QKO mice develop LCNEC with a predominant parenchymal location, whereas K5-QKO mice develop tumors mainly in proximal bronchi (Fig. 2*B*), similar to the corresponding human tumors.

We performed complete analyses in search of metastases and observed a different metastatic spreading. CMV-QKO mice did not develop any other pathology outside the lungs. In contrast, in liver and/or ganglia in 15 out of 31 analyzed K5-QKO mice, metastases were observed displaying histological features and neuroendocrine markers expression similar to primary lung tumors (Fig. 2*C*), resembling the metastatic behavior of human SCLC.

Altogether, these observations indicate that the tumors growing in the lung of CMV-QKO mice provide a robust model for LCNEC. The data also show that Ad5-K5cre–targeted basal cells can initiate SCLC tumors after suppression of *Rb1*, *Pten*, and *Trp53* in an *Rbl1*-null background, providing evidence that this specific cell type contributes to the development of SCLC.

Genomic Analysis of Mouse SCLC and Mouse LCNEC Tumors. To further characterize the LCNEC tumors arising from CMV-QKO (moLCNEC) and SCLC tumors arising from K5-QKO (moSCLC) mice, we performed whole-transcriptome analysis of mouse tumors and control (uninfected $Rb1^{F/F}$; $Rbl1^{-/-}$; $Trp53^{F/F}$; $Pten^{F/F}$) lung samples (moLung). The principal component analysis (PCA) of the transcriptomes showed that moLCNEC displayed high intragroup heterogeneity (Fig. 3*A* and *SI Appendix*, Fig. S4*A*) similar to that reported for human LCNEC (2–4). Among the 3 groups, moLung and moSCLC diverged the most along the principal component 1 (PC1) axis. The comparison of moSCLC or moLCNEC gene expression versus moLung (Fig. 3*B* and Dataset S2) confirmed this difference, supporting that the transcriptional impact of the *Rb1*, *Pten*, and *Trp53* gene deletion in the absence of *Rbl1* was greater in the moSCLC than in the moLCNEC. The up-regulated common genes to moLCNEC and moSCLC are primarily involved in cell cycle and mitotic progression (Fig. 3*C* and Dataset S3), consistent with the high mitotic rate of these tumors (Fig. 2*A*). Down-regulated genes in both tumors are involved in vasculogenesis and angiogenesis, as well as signaling pathways such as MAPK, TGF-beta receptor, BMP, PI3K, or NF-kappaB (*SI Appendix*, Fig. S4*B* and Dataset S3). moSCLC showed specific up-regulation of markers commonly found in human SCLC tumors, including neuroendocrine markers (ASCL1, CHGA, SCG3, NCAM1, SOX1, SYN1, SYP, ELAV3, ELAV4), while moLCNEC showed up-regulation of genes involved in immune response, keratinocyte differentiation (CALML3), and PHD3 (Egln3), an oxygen sensor recently involved in the modulation of metastasis and resistance to EGFR inhibitors in lung cancer (22) (Fig. 3*C* and Dataset S3). These data show significant

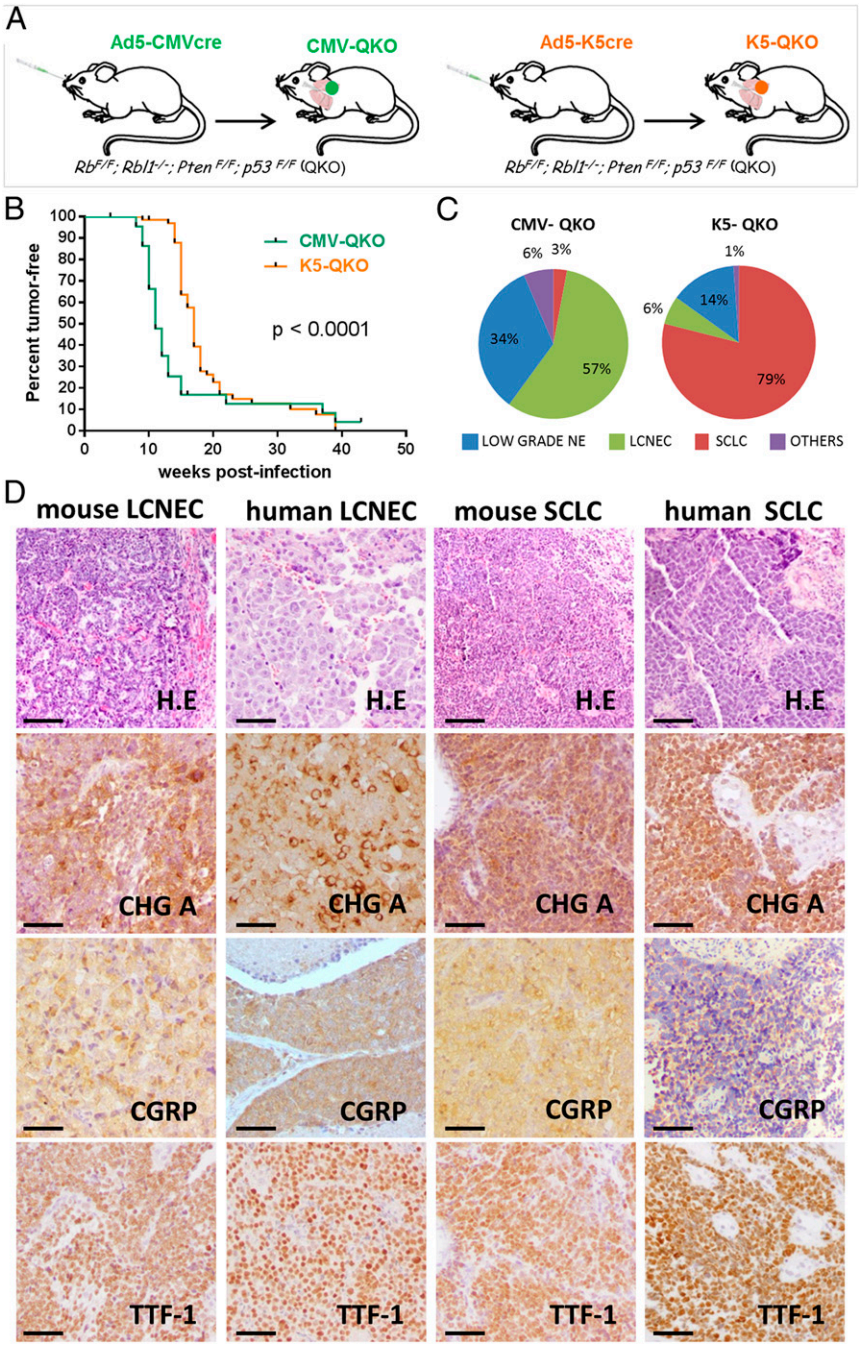

Fig. 1. Genetic deletion of 4 tumor suppressors in mouse lung epithelial cells results in LCNEC development. Basal cell-type restricted genetic deletion renders SCLC. (*A*) Schematic of mouse models experiment. *Rb1*$^{F/F}$;*Rbl1*$^{-/-}$;*Trp53*$^{F/F}$;*Pten*$^{F/F}$ (QKO) mice were infected with Ad5-CMVcre (CMV-QKO) or Ad5-K5cre (K5-QKO). (*B*) Kaplan-Meier percent tumor-free survival curve of *Rb1*$^{F/F}$;*Rbl1*$^{-/-}$;*Trp53*$^{F/F}$;*Pten*$^{F/F}$ mice infected with Ad5-CMVcre virus (green line) or Ad5-K5Cre virus (orange line). *x* axis: latency (weeks after adenovirus injection). Total number of mice analyzed for CMV-QKO, $n = 67$; K5-QKO, $n = 67$. (*C*) The pie charts represent the histopathology spectrum of tumors that arose from CMV-QKO or K5-QKO mice. Total number of tumors for CMV-QKO, $n = 886$; K5-QKO, $n = 537$. (*D*) Hematoxylin–eosin (H&E) representative images and immunohistochemical analyses of the quoted proteins in CMV-QKO LCNEC and human LCNEC (1st and 2nd panels) and K5-QKO SCLC and human SCLC (3rd and 4th panels). (Scale bars, 50 μm.) CHRA, Chromogranin A; CGRP, Calcitonin Gene Related Protein; TTF-1, Thyroid Transcription Factor-1; LCNEC, large-cell neuroendocrine carcinoma; SCLC, small-cell neuroendocrine carcinoma.

differences at the gene expression level. Since the set of genes deleted in both models is the same, these differences could be attributable to wide versus restricted cell-type targeting. Further analysis of these markers and molecular pathways could unveil relevant dissimilarities between these 2 types of high-grade neuroendocrine tumors.

Comparison of the 3 subtypes (moLung, moSCLC, and moLCNEC) with the well-established p53/Rb1 mouse model of SCLC described by Schaffer et al. (23) revealed a significant similarity between this model and our moSCLC tumors (*SI Appendix*, Fig. S5). Additionally, the moLung tumors associated with the Lung subclass in Shaffer's dataset (*SI Appendix*, Fig. S5), indicating that

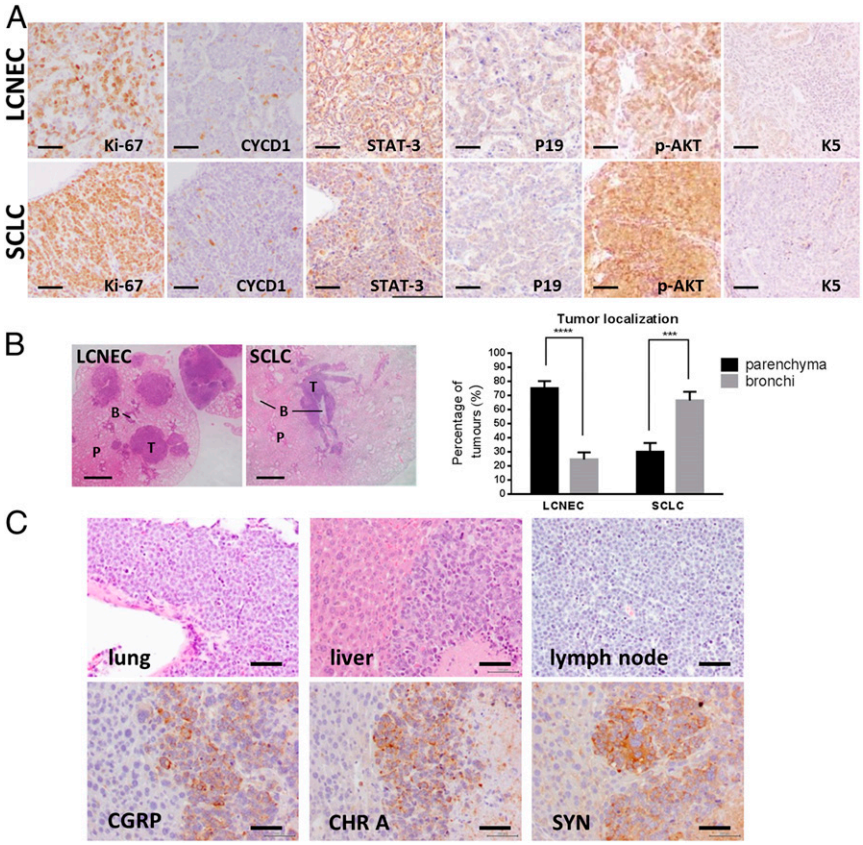

Fig. 2. Characterization of LCNEC and SCLC mouse tumors and metastasis. (*A*) Immunohistochemical analysis of LCNEC in CMV-QKO (*Top*) and SCLC in K5-QKO (*Bottom*) mice. Representative images of immunohistochemical staining for the quoted proteins. (Scale bars, 50 μm.) (*B*) Differential tumor growth localization in CMV-QKO and K5-QKO lungs. Representative images of H&E staining performed on lungs isolated from CMV-QKO mice (*Left*) with LCNEC growing in lung parenchyma and K5-QKO mice and (*Middle*) with SCLC growing lining bronchiole, respectively. P, parenchyma; B, bronchiole; T, tumor. Quantification of the comparison of parenchymal versus central tumor growth localization in Ad5-CMVcre and Ad5-K5cre-infected QKO mice (*Right*). Data represent mean ± SEM. ***P value = 0.0001 and ****P value ≤ 0.0001, determined by Mann–Whitney U test. (Scale bars, 1 mm.) (*C*) Development of metastases in K5-QKO mice. SCLC primary tumor in the lung (*Top Left*) of a K5-QKO mouse showing metastases in liver (*Top Middle*) and lymph node (*Top Right*). Immunohistochemical detection of the quoted neuroendcrine markers CGRP, Calcitonin Gene Related Protein (*Bottom Left*); CHRA, Chromoganin A (*Bottom Middle*); and SYN, synaptophysin in a liver metastasis of a K5-QKO mouse (*Bottom Right*). (Scale bars, 50 μm.)

the sole deletion of the *Rbl1* gene does not have a significant impact on gene expression in the normal lung.

Recently, a human LCNEC/SCLC classifier has been described that identifies 4 expression clusters termed classes I to IV, with LCNECs belonging mainly to classes I and II and SCLCs to classes III and IV (4). Unsupervised clustering analysis of the mouse tumors using the LCNEC/SCLC classifier identified 2 clusters of samples corresponding to the moLCNEC and the moSCLC (*SI Appendix*, Fig. S6*B*). The analysis of the LCNEC/SCLC classifier genes differentially expressed in moLCNEC versus moSCLC showed that the genes up-regulated in moLCNEC belong to genes up-regulated in class I and II expression clusters, while those up-regulated in moSCLC correspond to class IV up-regulated genes (Fig. 3*D*, *SI Appendix*, Fig. S6, and Dataset S4). Analysis of the enrichment in the moLCNEC and moSCLC expression datasets in genes specifically up- or down-regulated in classes I-IV further confirmed their similarity to human LCNEC and SCLC, respectively (*SI Appendix*, Fig. S6*C*).

Whole-exome analyses of the mouse tumors generated on average 28.3 million reads per tumor, and each base had 62.4× mean depth of coverage (Dataset S5). Mouse SCLC display higher mutation burden than LCNEC, although far below those reported in human tumors (12, 24) (28.4 and 8.6 transcript altering mutations on average per murine SCLC tumor and LCNEC tumor, respectively) (*SI Appendix*, Fig. S7 and Dataset S6). Transversions C:G > A:T were not as predominant as in human smoking-associated SCLC (12, 25); however, transitions seem to be of high prevalence in both groups (*SI Appendix*, Fig. S7). We found a total of 185 somatic alterations in 182 genes (Dataset S5). Some of the altered genes (Ahnak, Thsd7b, Lrrc61) were previously observed in other lung cancers. The reduced mutational burden (reported for SCLC mouse models [24, 26, 27]), together with the low prevalence of mutated genes in each group, suggests that the different tumor types arising in the 2 mouse groups are not due to specific divergent mutational evolution.

Copy number analysis showed more alterations in SCLC than in LCNEC (*SI Appendix*, Fig. S8); however, the alterations did not recreate in the different samples. Copy number variation hierarchical clustering of 10 tumor samples showed 2 main clusters; samples in each cluster are closed to each other and separated from the others. However, there were not special similarities among tumors of the same type and dissimilarities among tumors of different type, indicating that in terms of genomic copy number variations both types of tumor did not show differences.

Monitoring Tumors for Preclinical Testing with ^{18}FDG and ^{68}Ga-DOTATOC: Toward Early Lung Cancer Detection and Follow-up. The fact that the majority of patients with LCNEC and SCLC are diagnosed at advanced stages of the disease makes their therapeutic management particularly difficult. We aimed to develop

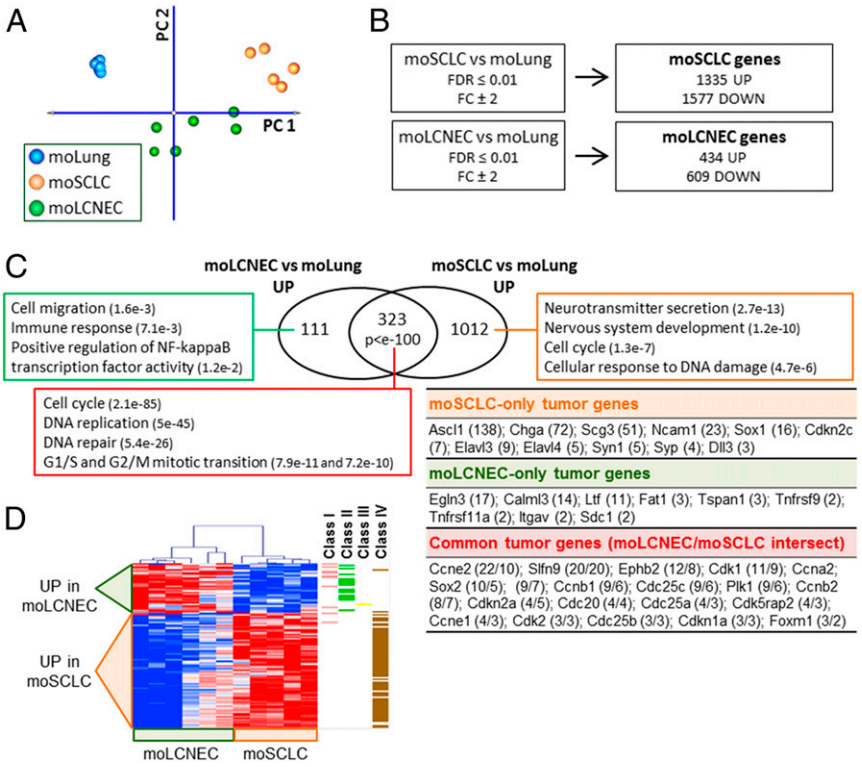

Fig. 3. Gene expression analyses of SCLC tumors arising from K5-QKO mice (moSCLC) and LCNEC tumors arising from CMV-QKO mice (moLCNEC). (*A*) PCA plot showing the distribution of the samples along PC1 and PC2. (*B*) Genes significantly (FDR ≤ 0.01) up-regulated or down-regulated more than 2-fold in moSCLC or in moLCNEC compared to lung. Numbers indicate Affymetrix probe set identifiers. FDR, false discovery rate; FC, fold change. (*C*) Venn diagram showing the overlap between the up-regulated genes in moSCLC versus moLung and moLCNEC versus moLung. Hypergeometric test was used to assess the statistical significance of the overlap. The rectangular boxes contain the main signaling pathways enriched in the indicated groups (gene ontology biological processes, category GEOTERM_BP_DIRECT). *P* values in brackets. The table shows some of the most relevant up-regulated genes in each group. Expression FC in brackets. In the case of common tumor genes: FC in moSCLC/FC in moLCNEC. (*D*) Heatmap representing the expression values of the LCNEC/SCLC classifier genes differentially expressed (*t* test, $P < 0.05$) in moLCNEC versus moSCLC (normalized gene/rows, unsupervised hierarchical clustering, Pearson correlation, average linking). Red and blue indicate high and low gene expression (−1 to 1 log2 gene expression value), respectively. Color clusters at the right side of the heatmap mark the genes specifically up-regulated in human LCNEC/SCLC clustering class (I-IV).

an early noninvasive in vivo method for lung cancer detection and follow-up assessment. Thus, taking advantage of the observed similarities to human samples, we performed combined microPET/computed tomography (CT) analyses in our mice.

Control noninfected ($n = 3$), as well as K5-QKO and CMV-QKO mice ($n = 10$) were imaged consecutively with ^{18}F-FDG and ^{68}Ga-DOTATOC. End-point histological analyses revealed the presence of SCLC ($n = 4$) and LCNEC ($n = 4$) tumors among K5-QKO and CMV-QKO mice, respectively. ^{18}F-FDG PET/CT failed to detect these tumors, whereas ^{68}Ga-DOTATOC PET/CT revealed areas of abnormally increased focal uptake as soon as 11 wk in K5-QKO mice (Fig. 4*A*), showing different standardized uptake value (SUV)max values that ranged from 0.79 to 2.74 (mean 1.77 ± 0.67). Immunohistochemistry confirmed the expression of SSTR2 in the tumors (Fig. 4*D*).

In K5-QKO and CMV-QKO mice, SCLC and LCNEC show clearly higher avidity for ^{68}Ga-DOTATOC than for ^{18}F-FDG. These data denote a remarkably higher sensitivity of the ^{68}Ga-DOTATOC for the detection of high-grade neuroendocrine tumors than the most widely used radiotracer ^{18}F-FDG. These studies show the feasibility of early detection of these tumors due to their avidity of ^{68}Ga-DOTATOC that allows follow-up and monitor changes after therapy. Unfortunately, the present data do not allow us to discern between LCNEC and SCLC tumor types but help to identify and differentiate both high-grade neuroendocrine tumors from other lung malignancies.

Discussion

Due to the notable paucity of human material from high-grade neuroendocrine lung tumors from surgery, preclinical mouse models emerge as essential tools for basic and translational research, in particular for LCNEC, since a robust, defined model for this cancer type has not been reported so far. Here we describe 2 accurate mouse models of LCNEC (CMV-QKO) and SCLC (K5-QKO) with unequivocal characteristics resembling their human counterparts. Recently, Gazdar and colleagues showed that some of the previously described models develop LCNEC to a minor extent (28), and Akeno et al. reported the formation of LCNEC along with SCLC (27). The CMV-QKO model presented in this study reveals that, in *Rbl1* knockout mice, the somatic inactivation of the tumor suppressors *Rb1*, *Pten*, and *Trp53* driven by Ad5-CMVcre leads to the formation of LCNEC with histopathological, molecular, and transcriptomic traits strikingly similar to human LCNEC (4). Ad5-CMVcre targeting of lung epithelial cells does not allow the identification of a specific cell type, if any, acting as a cell of origin of LCNEC. Nevertheless, the high incidence, uniform progression, and short latency period of the tumors in this immunocompetent model will facilitate the design and testing of novel tumor intervention strategies against LCNEC and can contribute to future research to identify the cellular origin of this tumor type.

In the QKO mice, Ad5-K5cre virus mediates recombination under steady state conditions in basal cells in which ablation of *Rb1*, *Pten*, and *Trp53* in an *Rbl1*-null background gives rise

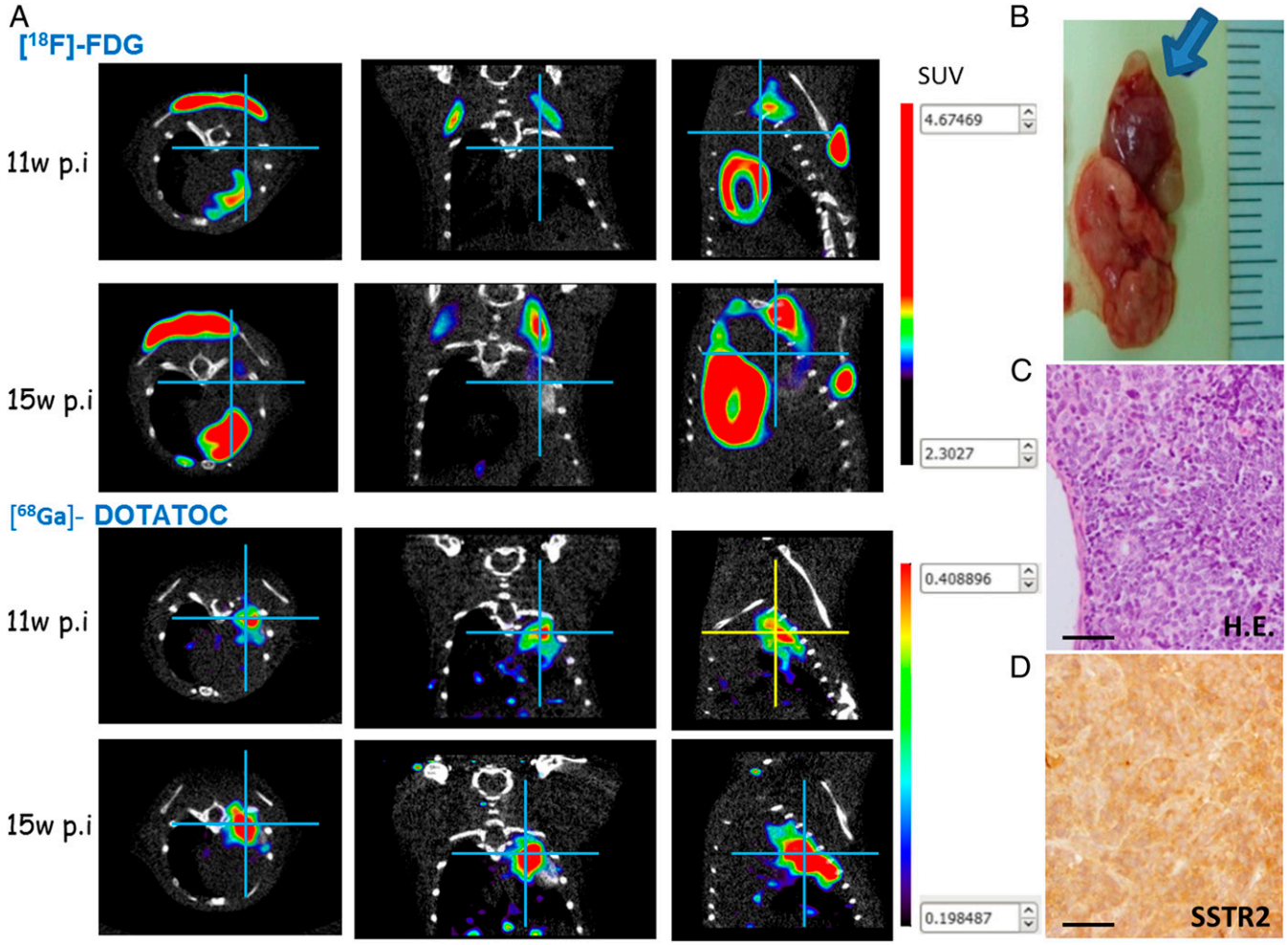

Fig. 4. Comparison of positron emission tomography (PET) imaging with ^{18}F-fluorodeoxyglucose (FDG) (*Top*) and ^{68}Ga-(tetraxetan-D-Phe1,Tyr3)-octreotide (DOTATOC) (*Bottom*). (*A*) Combined micro PET/CT images of a representative mouse K5-QKO. No increased ^{18}F-FDG utilization is observed in micro-PET in an animal with spontaneous SCLC, whereas a higher avidity for ^{68}Ga-DOTATOC is detected. (*B*) Gross tumor appearance of dissected lung (arrow). (*C*) H&E of the SCLC at necropsy. (*D*) Detection of SSTR2 by immunohistochemistry staining. (Scale bars, 50 μm.) w.p.i., weeks postinfection.

to lung tumors resembling human SCLC. Several studies have used different combinations of mutations required for SCLC development (mainly based on the *Trp53*/*Rb1* loss) and target widely (by using Ad5-CMVcre virus) or specifically (with Ad5-CGRPcre or Ad5-SPCcre virus) different respiratory epithelial cells, which define the lung lineages from which SCLC arises (reviewed in ref. 9). Among them, neuroendocrine cells have been identified as the predominant cell of origin in SCLC (29). Our K5-QKO model results in SCLC with very high frequency, homogeneity, and short latency, providing evidence that, in homeostatic conditions, keratin 5 expressing basal cells (that can demonstrably act as cell of origin of lung squamous cancer) (8) can give rise to SCLC. In support of this, primary basal epithelial cells can be transformed into small-cell neuroendocrine cancer (30). Taken together, these data confirm SCLC as a tumor type that arises from different cell types that profoundly influence its evolution (31). Additionally, different cell lineages are at the origin of adenocarcinoma (32) and squamous cell carcinoma (5), highlighting the plasticity of diverse putative cancer-initiating cells in the lung.

Reported mouse models show loss of Trp53 and Rb1 as a hallmark of SCLC, otherwise concurring with other genomic alterations (12, 25, 26). Our exome sequencing and CNV analysis did not show particular molecular features exclusive of any type of mouse tumor, and variants observed in our study would be mainly passenger mutations, thus reinforcing the role of the targeted cells in tumor evolution in the QKO mouse model.

In a similar approach, the *Rb1*, *Trp53*, *Pten* triple-knockout model has been used in 2 different studies, rendering either SCLC (1 Pten allele inactivation) or adenocarcinomas with neuroendocrine cell differentiation (both Pten alleles inactivated) when Ad5-CMVcre was used (25), or a mixture of LCNEC, SCLC and NSCLC when neuroendocrine cells were targeted using Ad-CGRPcre (28). Additional *Rbl1* loss renders LCNEC as the predominant tumor type in our CMV-QKO mice (Ad5-CMVcre) and SCLC in our K5-QKO mice (Ad5-K5cre), illustrating that both genetic alterations and characteristics of the initiated cells orchestrate the evolution of tumor phenotype (33). The fact that neuroendocrine tumors arise almost exclusively in both CMV-QKO and K5-QKO models highlights the ability of this gene to drive tumors to neuroendocrine phenotype (17). The extended animal survival of 17.5 wk in the Ad5-CMVcre Cui et al. model (25) versus 11 wk in the current CMV-QKO model shows that the additional loss of *Rbl1* accelerates tumor onset and supports a role for this gene as a tumor suppressor in lung cancer, as previously described in epidermal tumors (13–15). Interestingly, George et al. confirmed a role of RBL1 in the development of human SCLC (12), and the role of *Rbl2*, another

member of the Rb family, has been validated in an SCLC animal model (23).

^{68}Ga-DOTATOC provides a molecular-imaging system for neuroendocrine tumors. The absence of FDG uptake is an unexpected finding since these tumors are supposed to be ^{18}FDG-avid because of their high metabolic activity. However, in patients with SCLCs the SUVmax values for ^{18}F-FDG PET/CT can differ significantly, ranging from 1.18 to 25.99 (34). Moreover, in mice, measured SUV values in the lungs are greatly influenced by heart proximity to the selected region of interest. The lack of ^{18}F-FDG uptake in mice could be explained in part because of the different levels of the glucose transporter, GLUT-1, in pulmonary neuroendocrine tumors (35). As LCNEC and SCLC in CMV-QKO and K5-QKO transgenic mice seem to be ^{18}F-FDG negative, this work presents ^{68}Ga-DOTATOC as an alternative for early detection and monitoring of primary tumors. Unfortunately, we were not able to discern between LCNEC and SCLC tumors, but to discriminate them from other lung tumor types.

Collectively, our results indicate that the development of lung cancer subtypes appear to be, at least in mice, an interplay between targeted cell type and genotype. While the combination of genetic alterations is crucial for tumor development, this study illustrates the importance of the targeted cell/s in determining the type of high-grade neuroendocrine tumor. Furthermore, K5-QKO and CMV-QKO may provide accurate models of the human counterparts they resemble (SCLC and LCNEC, respectively) and a molecular imaging in vivo system for early detection and follow-up, ultimately tools for the design and testing of therapeutic intervention for diseases for which no optimal management has been found.

Materials and Methods

We used *Rb1*$^{F/F}$;*Rbl1*$^{-/-}$;*Pten*$^{F/F}$;*Trp53*$^{F/F}$ mice. Ablation of *Rb1*, *Trp53*, and *Pten* in pulmonary cells was achieved by intratracheal administration of 10^8 plaque-forming units of Ad5-CMVcre and Ad5-k5cre to 8- to 10-wk-old mice (16). All animal experiments were approved by the Animal Ethical Committee and conducted in compliance with CIEMAT guidelines. Characterization of tumors, in vivo noninvasive molecular-imaging system, and all other information regarding material and methods can be found in *SI Appendix*.

ACKNOWLEDGMENTS. We thank Dr. A. Hidalgo (Centro Nacional de Investigaciones Cardiovasculares) for kindly providing the ROSA26R-tdTomato mice, the personnel of the Animal Facility at CIEMAT for excellent care of the animals, and Norman Feltz for copyreading the manuscript. This study was funded by cofunded Fondo Europeo de Desarrollo Regional grants from Instituto de Salud Carlos III PI12/01959, PI15/00993, PI18/000263, Red Temática de Investigación Cooperativa en Salud RD12/0036/0009, and CIBERONC CB/16/00228; by Ministerio de Economía y Competitividad SAF2015-66015-R; and by PIE15/00076.

1. W. D. Travis *et al*.; WHO Panel, The 2015 world health organization classification of lung tumors: Impact of genetic, clinical and radiologic advances since the 2004 classification. *J. Thorac. Oncol.* **10**, 1243–1260 (2015).
2. N. Rekhtman *et al*., Next-generation sequencing of pulmonary large cell neuroendocrine carcinoma reveals small cell carcinoma-like and non-small cell carcinoma-like subsets. *Clin. Cancer Res.* **22**, 3618–3629 (2016).
3. T. Miyoshi *et al*., Genomic profiling of large-cell neuroendocrine carcinoma of the lung. *Clin. Cancer Res.* **23**, 757–765 (2017).
4. J. George *et al*., Integrative genomic profiling of large-cell neuroendocrine carcinomas reveals distinct subtypes of high-grade neuroendocrine lung tumors. *Nat. Commun.* **9**, 1048–1061 (2018).
5. A. Sánchez-Danés, C. Blanpain, Deciphering the cells of origin of squamous cell carcinomas. *Nat. Rev. Cancer* **18**, 549–561 (2018).
6. J. R. Rock *et al*., Basal cells as stem cells of the mouse trachea and human airway epithelium. *Proc. Natl. Acad. Sci. U.S.A.* **106**, 12771–12775 (2009).
7. D. T. Montoro *et al*., A revised airway epithelial hierarchy includes CFTR-expressing ionocytes. *Nature* **560**, 319–324 (2018).
8. G. Ferone *et al*., SOX2 is the determining oncogenic switch in promoting lung squamous cell carcinoma from different cells of origin. *Cancer Cell* **30**, 519–532 (2016).
9. E. A. Semenova, R. Nagel, A. Berns, Origins, genetic landscape, and emerging therapies of small cell lung cancer. *Genes Dev.* **29**, 1447–1462 (2015).
10. I. Kayani *et al*., A comparison of 68Ga-DOTATATE and 18F-FDG PET/CT in pulmonary neuroendocrine tumors. *J. Nucl. Med.* **50**, 1927–1932 (2009).
11. B. Venkitaraman, S. Karunanithi, A. Kumar, G. C. Khilnani, R. Kumar, Role of 68Ga-DOTATOC PET/CT in initial evaluation of patients with suspected bronchopulmonary carcinoid. *Eur. J. Nucl. Med. Mol. Imaging* **41**, 856–864 (2014).
12. J. George *et al*., Comprehensive genomic profiles of small cell lung cancer. *Nature* **524**, 47–53 (2015).
13. S. Ruiz *et al*., Unique and overlapping functions of pRb and p107 in the control of proliferation and differentiation in epidermis. *Development* **131**, 2737–2748 (2004).
14. M. F. Lara *et al*., p107 acts as a tumor suppressor in pRb-deficient epidermis. *Mol. Carcinog.* **47**, 105–113 (2008).
15. C. Costa *et al*., A novel tumor suppressor network in squamous malignancies. *Sci. Rep.* **2**, 828 (2012).
16. M. DuPage, A. L. Dooley, T. Jacks, Conditional mouse lung cancer models using adenoviral or lentiviral delivery of Cre recombinase. *Nat. Protoc.* **4**, 1064–1072 (2009).
17. S. Lázaro *et al*., Ablating all three retinoblastoma family members in mouse lung leads to neuroendocrine tumor formation. *Oncotarget* **8**, 4373–4386 (2017).
18. C. Rubio *et al*., CDK4/6 inhibitor as a novel therapeutic approach for advanced bladder cancer independently of RB1 status. *Clin. Cancer Res.* **25**, 390–402 (2019).
19. T. J. Lynch, J. F. Engelhardt, Progenitor cells in proximal airway epithelial development and regeneration. *J. Cell. Biochem.* **115**, 1637–1645 (2014).
20. L. Madisen *et al*., A robust and high-throughput Cre reporting and characterization system for the whole mouse brain. *Nat. Neurosci.* **13**, 133–140 (2010).
21. P. Soriano, Generalized lacZ expression with the ROSA26 Cre reporter strain. *Nat. Genet.* **21**, 70–71 (1999).
22. H. Dopeso *et al*., PHD3 controls lung cancer metastasis and resistance to EGFR inhibitors through TGFα. *Cancer Res.* **78**, 1805–1819 (2018).
23. B. E. Schaffer *et al*., Loss of p130 accelerates tumor development in a mouse model for human small-cell lung carcinoma. *Cancer Res.* **70**, 3877–3883 (2010).
24. M. Peifer *et al*., Integrative genome analyses identify key somatic driver mutations of small-cell lung cancer. *Nat. Genet.* **44**, 1104–1110 (2012).
25. M. Cui *et al*., PTEN is a potent suppressor of small cell lung cancer. *Mol. Cancer Res.* **12**, 654–659 (2014).
26. D. G. McFadden *et al*., Genetic and clonal dissection of murine small cell lung carcinoma progression by genome sequencing. *Cell* **156**, 1298–1311 (2014).
27. N. Akeno *et al*., TRP53 mutants drive neuroendocrine lung cancer through loss-of-function mechanisms with gain-of-function effects on chemotherapy response. *Mol. Cancer Ther.* **16**, 2913–2926 (2017).
28. A. F. Gazdar *et al*., The comparative pathology of genetically engineered mouse models for neuroendocrine carcinomas of the lung. *J. Thorac. Oncol.* **10**, 553–564 (2015).
29. K. D. Sutherland *et al*., Cell of origin of small cell lung cancer: Inactivation of Trp53 and Rb1 in distinct cell types of adult mouse lung. *Cancer Cell* **19**, 754–764 (2011).
30. J. W. Park *et al*., Reprogramming normal human epithelial tissues to a common, lethal neuroendocrine cancer lineage. *Science* **362**, 91–95 (2018).
31. D. Yang *et al*., Intertumoral heterogeneity in SCLC is influenced by the cell type of origin. *Cancer Discov.* **8**, 1316–1331 (2018).
32. K. D. Sutherland *et al*., Multiple cells-of-origin of mutant K-Ras-induced mouse lung adenocarcinoma. *Proc. Natl. Acad. Sci. U.S.A.* **111**, 4952–4957 (2014).
33. J. E. Visvader, Cells of origin in cancer. *Nature* **469**, 314–322 (2011).
34. S. J. Kim, S. Chang, Limited prognostic value of SUV max measured by F-18 FDG PET/CT in newly diagnosed small cell lung cancer patients. *Oncol. Res. Treat.* **38**, 577–585 (2015).
35. Y. S. Song *et al*., Correlation between FDG uptake and glucose transporter type 1 expression in neuroendocrine tumors of the lung. *Lung Cancer* **61**, 54–60 (2008).